Islamic Azad University

Journal of

Optoelectronical Nanostructures

Autumn 2020 / Vol. 5, No. 4

Investigation of Highly Broadb and Supercontinuum Generation in a Suspended As_2Se_3 Based Ridge Waveguide

Mohammad Reza Alizadeh[1], Mahmood Seifouri[*,1]

[1] Faculty of Electrical Engineering, Shahid RajaeeTeacher Training University, Tehran, Iran

(Received 3 Sep. 2020; Revised 11 Oct. 2020; Accepted 27 Nov. 2020; Published 15 Dec. 2020)

Abstract: In this paper, the generation of a highly broadband supercontinuum spectrum has numerically been investigated in a suspended As_2Se_3 based ridge waveguide. By changing the dimensions of the proposed waveguide, the dispersion has been engineered to achieve a suitable profile with the two zero-dispersion wavelengths as well as the lower magnitude and flat anomalous dispersion regime. Due to the high refractive index contrast between the core and cladding, the propagated light has been highly confined in the core and as a result, a high optical nonlinear coefficient has been obtained. Simulation results show that when the pump pulses with a width of 100 fs and peak power of 1KW at the wavelength of 2150 nm are injected into the designed waveguide with a length of 0.8 mm, the generated supercontinuum can be broadened in the wavelength range from 1.4 to 18μm. Such a waveguide structure is highly applicable for on-chip mid-infrared supercontinuum sources that are very important in many fields such as optical coherence tomography, fingerprint, molecular spectroscopy, and else.

Keywords: Supercontinuum Generation, Dispersion, Ridge Waveguide, Zero-Dispersion Wavelength, Highly Nonlinear.

1. INTRODUCTION

Mid-infrared (MIR) supercontinuum generation (SCG) is of immense interest because of its many applications in different fields such as molecular spectroscopy, optical coherence tomography, frequency metrology, pulse compression, fingerprinting, biochemical sensing, and so on. The supercontinuum (SC) spectrum is the broadening of very short pulses that are injected into the input of a waveguide. It can be generated from the interaction of various nonlinear and linear optical effects, including self-phase modulation (SPM), cross-phase modulation (XPM), four-wave mixing (FWM), stimulated

* Corresponding author. Email: **Mahmood.Seifouri@sru.ac.ir**

Raman scattering (SRS), self-steepening (SS), soliton dynamics (SD), and dispersive waves (DW) [1–10].

The weak nonlinearity of silica-based structures requires a pumping source with high peak power for SCG. Additionally, due to the high material absorption of the silica materials in the mid-infrared (MIR) wavelength range, they have limitations for the spectral broadening in this region. By comparison, the chalcogenide glasses (ChGs) can be potential candidates to overcome the mentioned limitation of silica glasses. They consist of chalcogen elements such as S, Se, and Te (the Group 16 of the periodic table of elements) combined with other elements such as Si, As, Ge, P, and Sb. Due to their optical transparency up to 25 μm in the infrared domain, ChGs can be used for mid-infrared supercontinuum generation[11-12]. In addition, they show high Kerr nonlinearity as well as low two-photon absorption (TPA) and as a result, ChGs are very useful for SCG.

Numerous theoretical and experimental investigations have focused on SCG using silica, tellurite, fluoride, silicon, and chalcogenide glasses based step-index fibers, photonic crystal fibers (PCFs), and waveguides[13-20]. In recent years, planar waveguides have attracted much attention, due to their short interaction length, scalable, more robust, and compact structure, and low cost integrated optical chip fabrication in comparison with the SC generation from photonic crystal fibers[21-36].

In this paper, we have designed a suspended As_2Se_3 ridge waveguide for a highly coherent and on-chip SCG in the M−IR region. In this structure, the As_2Se_3 layer is suspended above the MgF_2 substrate with a thick air gap that causes a much larger refractive index contrast, resulting in a stronger mode field confinement. The numerical investigation shows that the designed ridge waveguide structure has an engineered dispersion profile with the two zero-dispersion wavelengths (ZDWs) where the pump pulses have been injected into the anomalous dispersion region. We have studied the effects of the input pulse parameters including peak power, pulse width, and its wavelength on the output spectrum. Moreover, the effect of different waveguide lengths on SCG has been demonstrated.

2. WAVEGUIDE DESIGN AND CHARACTERISTICS

Figure 1 shows the cross-section of our proposed suspended ridge waveguide geometry in which the As_2Se_3 channel is suspended above the SiO_2 substrate and there is a thick air gap between them.

For the confinement of the propagation of the light field into the As_2Se_3 core, the top of this layer has been designed as air cladding. By covering the As_2Se_3 layer with air, the proposed structure shows strong-mode field confinement because of a much larger refractive index contrast. The height of the slab layer has been h_2, while the width and height of the ridge core have been W_1 and h_1,

respectively. By etching the SiO_2 substrate, we have provided enough space with a thickness of 2 µm between the As_2Se_3 and SiO_2 layers. The geometry has been simulated by using a wavelength-dependent linear refractive index that can be calculated through the following Sellmeier equation.

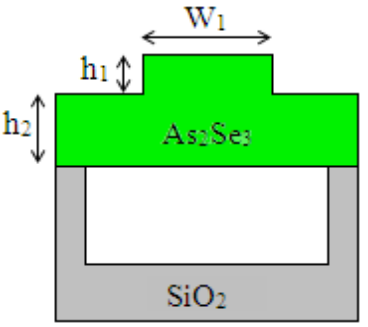

Fig. 1. Cross-section of the designed As_2Se_3 based ridge waveguide with SiO_2 substrate.

For the confinement of the propagation light field into the As_2Se_3 core, the top of this layer is designed as air cladding. By covering the As_2Se_3 layer with air, proposed structure shows a strong mode field confinement because of a much larger refractive index contrast. The height of the slab layer is h_2, while the width and height of the ridge core are W_1 and h_1, respectively. By etching the SiO_2 substrate, we provide enough space with thickness of 2 µm between the As_2Se_3 and SiO_2 layers. The geometry was simulated by using wavelength-dependent linear refractive index that can be calculated through the following Sellmeier equation.

$$n(\lambda)=\left[1+\lambda^2\left[A_1^2/\left(\lambda^2-B_1^2\right)+A_2^2/\left(\lambda^2-B_2^2\right)+A_3^2/\left(\lambda^2-B_3^2\right)\right]\right]^{0.5} \quad (1)$$

The values of A_1, A_2, A_3, B_1, B_2, and B_3 for used glasses have been presented in the following table[17, 28, 37].

TABLE I
SELLMEIER COEFFICIENTS FOR BOTH As_2Se_3 AND SiO_2

Material	As_2Se_3		SiO_2	
	A_i	B_i	A_i	B_i
i=1	0.24164	0.24164	0.696166300	0.004679148
i=2	0.347441	19	0.407942600	0.013512063
i=3	1.308575	0.48328	0.897479400	97.93400250

3. THEORY

To study the evolution of the short pulses in the proposed waveguide, the generalized nonlinear Schrödinger equation (GNLSE) must be solved

numerically using the split-step Fourier method. The simplified form of this equation has been presented below [38]:

$$(\partial \mathrm{A}/\partial \mathrm{Z}) = (D+N)A \tag{2}$$

In this equation, D and N indicate the linear and nonlinear parts of the equation, respectively. The value of D has been presented as follows[39, 40].

$$D = -(\alpha(\omega)/2) + \sum_{n\geq 2} \beta_n \left(i^{n+1}/\beta_n!\right)\left(\partial^n/\partial t^n\right) \tag{3}$$

Where α is the loss factor that can be neglected due to the low waveguide length. $\beta_n(n \geq 0)$is the m-order dispersion coefficient that is obtained by the following equation[40].

$$\beta_m = \left(d^m \beta / d\omega^m\right)_{\omega=\omega_0} (m = 0,1,2,\ldots) \tag{4}$$

Where ω_0 represents the reference frequency. It is very useful to calculate the high orders of dispersion that are computed up to the tenth order in our simulation. In addition, the nonlinear part of the equation has been defined as follows[41]:

$$N = i\gamma\left(1 + (i/\omega_0)(\partial/\partial t)\right) \int_{-\infty}^{\infty} R(T') \left|A(Z, T-T')\right|^2 dT' \tag{4}$$

Where A indicates the input electric field envelope and γ is the nonlinear parameter of the waveguide that is defined by the following equation:

$$\gamma = \left(\omega_0 n_2 / c A_{eff}\right) = 2\pi n_2 / \lambda_0 A_{eff} \tag{5}$$

Where λ_0 represents center wavelength, n_2 is the nonlinear Kerr index of the glass material used in the waveguide's core, and A_{eff} represents the wavelength dependence effective mode area.

Additionally, in equation (6), $R(T')$ is the nonlinear Raman response function and can be represented as follows [42].

$$R(T') = (1 - f_R)\delta(T) + f_R h_R(T) \tag{6}$$

Where $f_R = 0.115$ and $h_R(T)$ is the delayed Raman response function obtained by the following equation:

$$h_R(T) = \left(\left(\tau_1^2 + \tau_2^2\right)/\left(\tau_1^2 \tau_2^2\right)\right) exp(-t/\tau_2) sin(t/\tau_1) \tag{7}$$

Where $\tau_1 = 23\times10^{-15}$s is the phonon oscillation frequency and $\tau_2 = 195\times10^{-15}$s is the characteristic damping time of atoms vibration related to As_2Se_3[8]. Using the following equation, the chromatic dispersion parameter $D(\lambda)$ has been related to the group velocity dispersion (GVD) or β_2. Additionally, using equation (8), one can calculate the propagating mode of wavelength-dependent effective refractive index by employing the full-vector finite-element method [8].

$$D(\lambda) = -(\lambda/c)\left[\partial^2 \mathrm{Re}(n_{eff})/\partial\lambda^2\right] \quad (8)$$

Where, c and n_{eff} are the light velocity in a vacuum and the waveguide's effective index, respectively.

4. EXAMINATION OF DISPERSION AND OPTIMIZATION

By employing the full-vector finite-element method, we have calculated the n_{eff} of the waveguide. Then, using equation (9), the chromatic dispersion has been calculated as a function of the wavelength. The dispersion profiles can be optimized by the domination of the waveguide with different geometrical parameters.

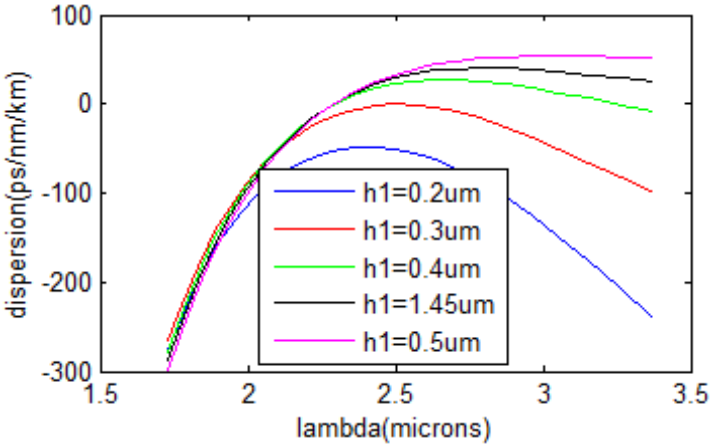

Fig. 2. Variations in dispersion profile by increase of h_1 as functions of wavelength.

The generation of SC and its expansion depends critically on the group-velocity dispersion (GVD) profile and its optimization. By pumping the input pulse in an anomalous dispersion regime with a low GVD value and in the vicinity of the zero-dispersion wavelength (ZDW), one can generate efficient broadband SC. To achieve suitable ZDW, the waveguide geometries must be optimized. In this part, we have investigated the effects of the changes of ridge As_2Se_3 layer

geometry on the dispersion profile. The results obtained regarding the effects of the waveguide geometry variation on GVD have been shown in figures 2-4.

In Fig. 2, the variations in the dispersion profile by the increase in h_1 have been shown. When the value of h_1 is 0.45 and 0.5μm, the dispersion profile remains in the normal dispersion region. If h_1 is lower than 0.4μm, the anomalous dispersion region increases with the increase in h_1. The second ZDW is created and shifts to taller wavelengths when h_1 decreases.

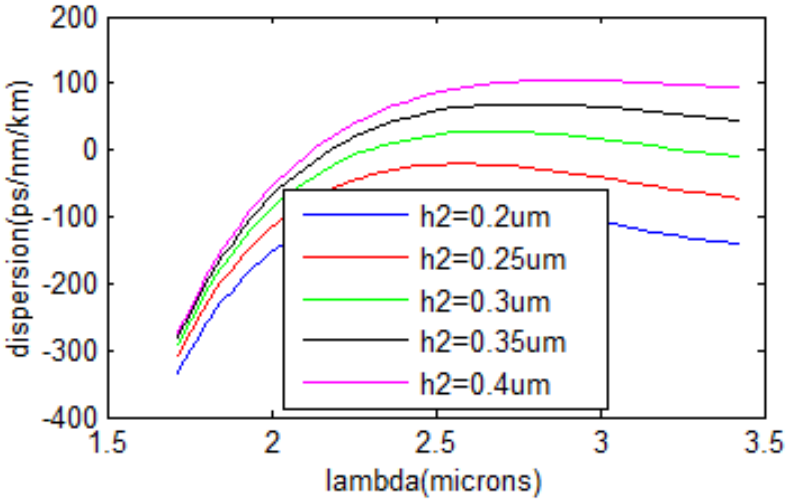

Fig. 3. variations in dispersion profile by increase of h_1 as functions of wavelength.

In fig.3, we have also plotted the dispersion profile variation by increasing h_2. As shown in this figure, by increasing h_2 to higher than 0.3μm, the anomalous dispersion region appears and increases with the increase in h_2.

In fig.4, the effects of variations in w_2 on the dispersion profile have been shown. In the case where w_2 is 1.2 and 1.4μm, the profile is located completely in the normal dispersion region. However, in the case of w_2 = 1.6μm, the curve is flatter and includes low anomalous dispersion, and the two zero-dispersion wavelengths are created around the wavelengths of 2.2μm and 3.3μm. When the value of w_2 is 1.7 and 1.8 μm, there are still the two zero-dispersion wavelengths, but the amount of dispersion is high in the anomalous region.

As seen in the above figures, the dispersion profile is very sensitive to w_2, h_1, and h_2. The second ZDW shows a red shift by increasing w_2, h_1, and h_2. In addition, by increasing them, the value and region of the anomalous dispersion gradually increase. For extending SC in a very high wavelength, it is necessary

to inject the input pump pulse into the anomalous dispersion region and close to the first ZDW. According to the above analysis, we have optimized the proposed structure by setting up w_2=1.6µm, h_1=0.4 µm, and h_2=0.3 µm.

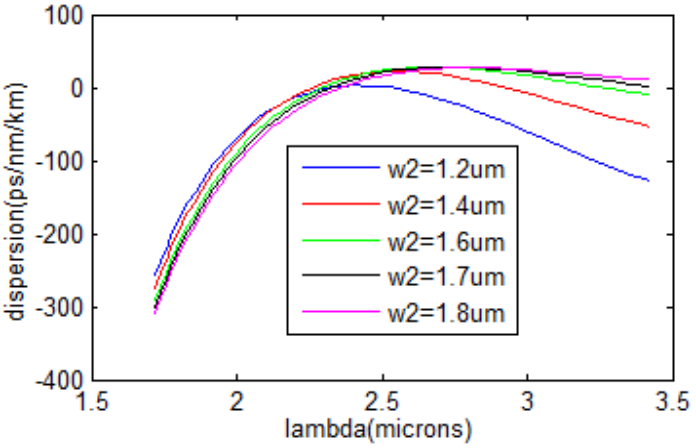

Fig. 4. variations in dispersion profile by increase of w_1 as functions of wavelength.

5. THE SUPERCONTINUUM GENERATION

For SC generation in the proposed structure, the Schrödinger equation presented as equation (2) has numerically been solved using the split-step Fourier method. As discussed earlier, a broadband SCG can be achieved using a pump pulse with a wavelength close to the ZDW of the waveguide.

It should be noted that the nonlinear coefficient of the proposed ridge waveguide has been 86.1 W^{-1} m^{-1} with an effective mode area of 0.8 μm^2 at 2150 nm. In the following, we have investigated the effects of the pump pulse parameters including pump wavelength, pulse duration, input peak power, and proposed ridge waveguide length on SCG. In the first step, we have changed pump wavelengths from 2.1 to 3.05 µm and used pump pulse with the peak power of 1kw and the width of 100fs. As shown in fig.5, the output spectrum is suitable in the case of 2.15µm.

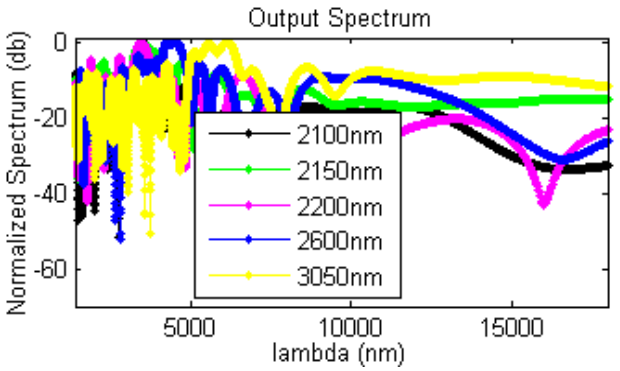

Fig. 5. Investigation of the influences of the pump wavelengths on the output spectrum

Then, we have studied the effect of peak power on the SCG. The output spectral profiles have been shown in fig. 6 when the peak power of the pump pulse at 2.15µm with the width of 100 fs has been changed from 500w to 1kw. It can be observed that the corresponding bandwidth of the generated SC can be enhanced by increasing the input peak power to 1kw.

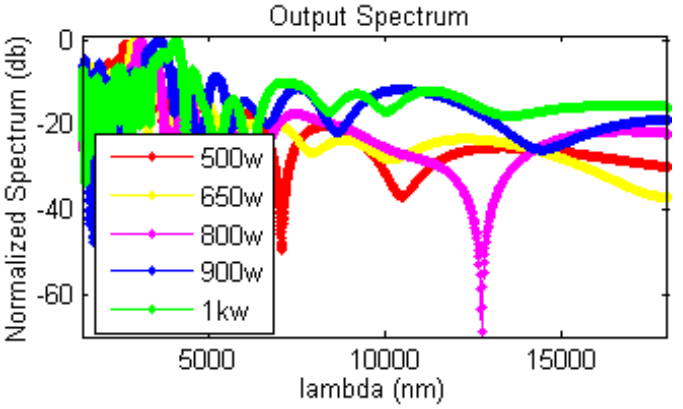

Fig. 6. Effects of variations in input pump power from 500w to 1kw on SCG expansion.

Additionally, we have investigated the effect of the pump pulse widths of 50, 100, and 150 fs on SCG. As seen in fig. 7, the pump pulse with a width of 100 fs is more suitable for the generation of broadband SC spectrum.

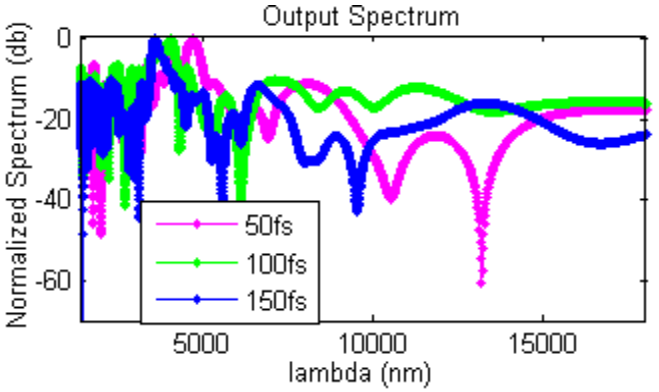

Fig. 7. Effects of variations in input pump pulses widths on SCG expansion.

Fig. 8 shows the spectral broadening of the generated SC with various lengths of the proposed ridge waveguide. As shown in this figure, the extension of the broad coherent SC spectrum from 1.4 to 18 µm has been achieved with a waveguide length of 0.8mm, pump pulse at 2.15µm with the width of 100fs, and the peak power of 1kw. Fig. 9 shows the final SCG with optimized pump pulse parameters as discussed above.

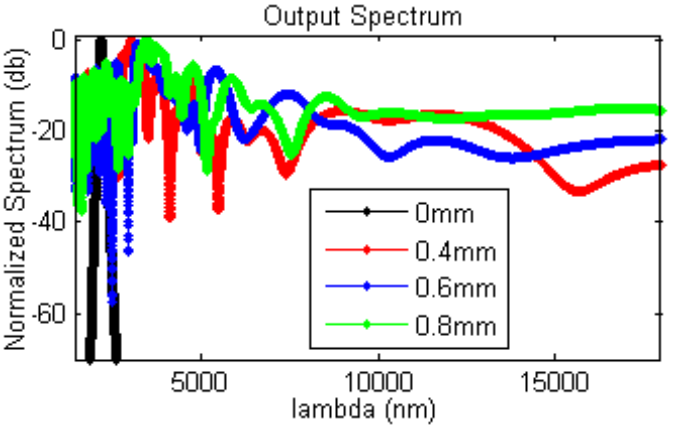

Fig. 8. Effects of variations in input pump pulses widths on SCG expansion.

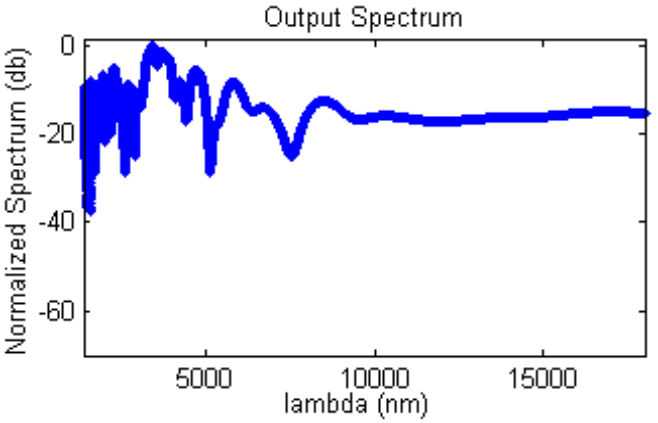

Fig. 9. Final generated SC spectra in the waveguide with length of 0.8mm, peak power of 1kw, and pump pulse width 100 fs in 2.15µm.

As shown in fig. 9, by numerical simulation in this paper, the broaden SCG extension from 1.4 to 18µm has been achieved in ridge waveguide length of 0.8mm with the peak power of 1kw and the pulse width of 100 fs at 2.15µm.

6. CONCLUSION

In summary, we have numerically modeled an As_2Se_3 based ridge waveguide with the two ZDWs for the broadband supercontinuum generation. We have also investigated the effects of the pump pulse parameters and waveguide length on the generated SC spectrum. Using pump pulse at the wavelength of 2.15µm with the peak power of 1 kw and the pulse width of 100fs in the waveguide length of 0.8 mm, an ultra-flat broadband SCG extension from 1.4 to 18µm has been achieved.

Such proposed waveguide is suitable for being used in integrated optical circuits with potential applications in spectroscopy, cancer detection, medical imaging, pulse compression, gas sensing, optical coherence tomography, fingerprinting, and metrology.

REFERENCES

[1] *Mid-infrared laser applications in spectroscopy*, Mid-infrared laser applications in spectroscopy, in Handbook of Solid-State Mid-Infrared Laser Sources, Springer F. K. Tittel, D. Richter, and A. Fried, 2003.

[2] S. Haxha and H. Ademgil. *Novel design of photonic crystal fibers with low confinement losses, nearly zero ultraflattened chromatic dispersion, negative chromatic dispersion and improved effective mode area*. Opt. Commun 281 (2008) 278–286. Available: https://doi.org/10.1016/j.optcom.2007.09.041

[3] I. Hartl, X. D. Li, C. Chudoba, R. K. Ghanta, T. H. Ko, J. G. Fujimoto, J. K. Ranka, and R. S. Windeler. *Ultrahigh-resolution optical coherence tomography using continuum generation in an air-silica microstructure optical fiber*. Opt. Lett. 26 (2001) 608–610.
Available: https://link. springer.com/chapter/10.1007/ 978-3-642-56546-5_73

[4] A. Schliesser, N. Picque, and T. W. Hansch. *Mid-infrared frequency combs*. Nat. Photonics 6 (2012) 440–449.
Available: https://doi.org/10.1038/nphoton.2012.142

[5] I. D. Aggarwal and J. S. Sanghera. *Development and application of chalcogenide glass optic fiber at NRL*. J. Optoelectron. Adv. Mater 4 (2002) 665–678. Available: https://doi.org/10.1016/S0022-3093(97)00051-3

[6] A. V. Husakou and J. Herrmann. *Supercontinuum generation of higher-order solitons by fission in photonic crystal fibers*. Phys. Rev. Lett. 87 (2001) 203901. Available: https://doi.org/10.1103/PhysRevLett.87.203901

[7] J. M. Dudley, G. Genty, and S. Coen. Supercontinuum generation in photonic crystal fiber. Rev. Mod. Phys 78 (2006) 1135–1184.
Available: https://doi.org/10.1103/RevModPhys.78.1135

[8] G.P. Agrawal, Nonlinear Fiber Optics, 5th ed., Elsevier Academic Press, 2013.

[9] P. Russell. *Photonic crystal fibers*. Science 299 (2003) 358–362.
Available: 10.1126/science.1079280

[10] J.M. Dudley, J.R. Taylor, *Supercontinuum generation in optical fibers*, Cambridge University Press, 2010.

[11] B. J. Eggleton, B. L. Davies, and K. Richardson. *Chalcognide photonics*. Nature Photon. 5 (2011) 141 – 148.
Available: https://doi.org/10.1038/nphoton.2011.309

[12] V. Shiryaev and M. Churbanov. *Trends and prospects for development of chalcogenide fibers for mid-infrared transmission.* J. Non-Cryst. Solids 377 (2013) 225 – 230. Available: https://doi.org/10.1016/j.jnoncrysol.2012.12.048

[13] J. Hu, C.R. Menyuk, L.B. Shaw, J.S. Sanghera, I.D. Aggarwal. *Maximizing the bandwidth of supercontinuum generation in As_2Se_3 chalcogenide fibers.* Opt. Express 18 (2010) 6722–6739.
Available: 10.1364/oe.18.006722

[14] T.S. Saini, A. Baili, A. Kumar, R. Cherif, M. Zghal, R.K. Sinha. *Design and analysis of equiangular spiral photonic crystal fiber for M-IR supercontinuum generation*. Journal Modern Optics 62 (2015) 1570–1576.

Available: https://doi.org/10.1080/09500340.2015.1051600

[15] F. Xu, J. Yuan, C. Mei, B. Yan, X. Zhou, Qi. Wu, K. Wang, X. Sang, C. Yu, G. Farrell. *Highly coherent supercontinuum generation in a polarization-maintaining CS_2-core photonic crystal fiber*. Applied Optics 58 (6) (2019) 1386–1392. Available: 10.1364/AO.58.001386

[16] A. Medjouri, D. Abed, Z. Becer. *Numerical investigation of a broadband coherent supercontinuum generation in $Ga_8Sb_{32}S_{60}$ chalcogenide photonic crystal fiber with all-normal dispersion.* Opto-Electronics Review 27 (1) (2019) 1–9. Available: https://doi.org/10.1016/j.opelre.2019.01.003

[17] M. Seifouri, M.R. Alizadeh. *Supercontinuum generation in a highly nonlinear chalcogenide/MgF_2 hybrid photonic crystal fiber.* International Journal of Optics and Photonics 12 (1) (2018) 69–78.
Available: http://ijop.ir/article-1-277-en.html

[18] H. Balani, G. Singh, M. Tiwari, V. Janyani, A.K. Ghunawat. *Supercontinuum generation at 1.55 μm in As_2S_3 core photonic crystal fiber.* Applied Optics 57 (13) (2018) 3524–3533.
Available: https://doi.org/10.1364/AO.57.003524

[19] M.R. Karim, H. Ahmad, S. Ghosh, B.M.A. Rahman. *M-IR supercontinuum generation using As_2Se_3 photonic crystal fiber and the impact of higher-order dispersion parameters on its supercontinuum bandwidth*. Optical Fiber Technology 45 (2018) 255–266. Available: https://doi.org/10.1063/1.5033494

[20] S. Kalra, S. Vyas, M. Tiwari, G. Singh, *Multi-material photonic crystal fiber in M-IR region for broadband supercontinuum generation*. Optical and Wireless Technologies. Springer (2018) 199–209.
Available:https://www.springerprofessional.de/en/multi-material-photonic-crystal-fiber-in-mir-region-for-broadban/15460216

[21] Bing-Xi Xiang, Lei Wang, Yu-Jie Ma, Li Yu, Huang-Pu Han, Shuang-Chen Ruan. *Supercontinuum Generation in Lithium Niobate Ridge Waveguides Fabricated by Proton Exchange and Ion Beam Enhanced Etching.* CHIN. PHYS. LETT 34(2) (2017) 024203.
Available: https://doi.org/10.1088/0256-307X/34/2/024203

[22] J. M. Morris, M. D. Mackenzie, C. R. Petersen, G. Demetriou, A. K. Kar, O. Bang, and H. T. Bookey. *$Ge_{22}As_{20}Se_{58}$ glass ultrafast laser inscribed waveguides for mid-IR integrated optics*. Opt. Mater. Express 8 (2018) 1001–1011. Available: https://doi.org/10.1364/OME.8.001001

[23] N. Singh, D. D. Hudson, Y. Yu, C. Grillet, S. D. Jackson, A. Casas- Bedoya, A. Read, P. Atanackovic, S. G. Duvall, S. Palomba, B. Luther-Davies, S.

Madden, D. J. Moss, and B. J. Eggleton. *Midinfrared supercontinuum generation from 2 to 6 lm in a silicon nanowire.* Optica 2 (2015) 797–802. Available: https://doi.org/10.1364/OPTICA.2.000797

[24] T. S. Saini, A. Kumar, and R. K. Sinha. *Design and modelling of dispersion-engineered rib waveguide for ultra broadband mid-infrared supercontinuum generation.* J. Mod. Opt. 64 (2016) 143–149. Available: https://doi.org/10.1080/09500340.2016.1216190

[25] Y. Yu, X. Gai, P. Ma, K. Vu, Z. Yang, R. Wang, D. Choi, S. Madden, and B. Luther-Davies. *Experimental demonstration of linearly polarized 2–10μm supercontinuum generation in a chalcogenide rib waveguide.* Opt. Lett. 41 (2016) 958–961. Available: 10.1364/OL.41.000958

[26] T. S. Saini, N. P. T. Hoa, K. Nagasaka, X. Luo, T. H. Tuan, T. Suzuki, and Y. Ohishi. *Coherent midinfrared supercontinuum generation using a rib waveguide pumped with 200 fs laser pulses at 2.8 μm.* Appl. Opt. 57 (2018) 1689–1693. Available: 10.1364/AO.57.001689

[27] T. S. Saini, U. K. Tiwari, and R. K. Sinha. *Design and analysis of dispersion engineered rib waveguides for on-chip mid-infrared supercontinuum*. J. Lightwave Technol. 36 (2018) 1993–1999. Available: https://www.osapublishing.org/jlt/abstract.cfm?URI=jlt-36-10-1993

[28] T. S. Saini, U. K. Tiwari, and R. K. Sinha. *Rib waveguide in Ga-Sb-S chalcogenide glass for on-chip mid-IR supercontinuum sources: Design and analysis*. J. Appl. Phys. 122(5) (2017) 053104. Available: 10.1063/1.4997541

[29] X. Gai, D.-Y. Choi, S. Madden, Z. Yang, R. Wang, and B. Luther- Davies. *Supercontinuum generation in the mid-infrared from a dispersion-engineered As_2S_3 glass rib waveguide.* Opt. Lett. 37 (2012) 3870–3872. Available: https://doi.org/10.1364/OL.37.003870

[30] Y. Yu, X. Gai, T. Wang, P. Ma, R. Wang, Z. Yang, D. Y. Choi, S.Madden, and B. L. Davies. *Mid-infrared supercontinuum generation in chalcogenide*. Opt. Mat. Express 3(8) (2013) 1075 – 1086. Available: https://doi.org/10.1364/OME.3.001075

[31] M. R. Karim, B. M. A. Rahman, and G. P. Agrawal. *Mid-infrared superccontinuum generation using dispersion-engineered $Ge_{11.5}As_{24}Se_{64.5}$ chalcogenide channel waveguide.* Opt. Exp. 23(5) (2015) 6903 – 6914. Available: https://doi.org/10.1364/OE.23.006903

[32] J. W. Choi, Z. Han, B-Uk. Sohn, G. F. R. Chen, C. Smith, L.C.Kimerling, K. A. Richardson, A. M. Agarwal, and D. T. H. Tan. *Nonlinear*

characterization of GeSbS chalcogenide glass waveguides. Sci. Rep. 6 (2016) 39234 - 3923. Available: 10.1038/srep39234

[33] T. S. Saini, A. Kumar, and R. K. Sinha. *Design and modeling of dispersion engineered rib waveguide for ultra-broadband mid-infrared supercontinuum generation.* J. Mod. Opt. 64 (2017) 143–149. Available: https://doi.org/10.1080/09500340.2016.1216190

[34] M.R. Alizadeh , M. Seifouri. *Dispersion engineering of highly nonlinear rib waveguide for mid-infrared super continuum generation.* Optik 140 (2017) 233–238. Available: https://doi.org/10.1016/j.ijleo.2017.04.056

[35] M. R. Karim, H. Ahmad, S. Ghosh, and B. M. A. Rahman. *Design of dispersion-engineered As_2Se_3 channel waveguide for mid-infrared region supercontinuum generation.* J. Appl. Phys. 123 (2018) 213101. Available: https://doi.org/10.1063/1.5033494

[36] M.R. Alizadeh , M. Seifouri. *Design and Analysis of a Dispersion-engineered and Highly Nonlinear Rib Waveguide for Generation of Broadband Supercontinuum Spectra.* Frequenz 74 (3-4) (2019) 153–161. Available: https://doi.org/10.1515/freq-2019-0098

[37] Zeli Li, Jinhui Yuan, Chao Mei, Feng Li, Xian Zhou, Binbin Yan, Qiang Wu, Kuiru Wang, Xinzhu Sang, Keping Long, AND Chongxiu Yu. *Multi-octave mid-infrared supercontinuum and frequency comb generation in a suspended As_2Se_3 ridge waveguide.* Applied Optics 58 (31) (2019) 8404-8410. Available: 10.1364/AO.58.008404

[38] M.R. Karim, B.M.A. Rahman. *Ultra-broadband mid-infrared supercontinuum generation using chalcogenide rib waveguide.* Opt. Quant. Electron. 48 (2016) 174. Available: https://doi.org/10.1007/s11082-016-0458-5

[39] M. Yang, Y. Guo, J. Wang, Z. Han, K. Wada, L. C. Kimerling, A. M. Agarwal, J. Michel, G. Li, and L. Zhang. *Mid-IR supercontinuum generated in low dispersion Ge-on-Si waveguides pumped by sub-ps pulses.* Opt. Express 25 (2017) 16116–16122. Available: https://doi.org/10.1364/OE.25.016116

[40] Z. Zho, T. Brown. *Full-vectorial finite-difference analysis of microstructure optical fibers*. Opt. Express 10 (85) (2002) 53–64. Available: https://doi.org/10.1364/OE.10.000853

[41] C. Ming, Y. Qing, L. Tiansong, C. Mingsong, H. Ning. *New high negative dispersion photonic crystal fiber.* New Optik 121 (2010) 867–871. Available: https://doi.org/10.1016/j.ijleo.2008.09.039

[42] Tomasz Karpisz, Bartlomiej Salski, Anna Szumska, Mariusz Klimczak, Ryszard Buczynski. *FDTD analysis of modal dispersive properties of nonlinearphotonic crystal fibers*. Opt. Quant. Electron. 47 (2015) 99–106. Available: https://doi.org/10.1007/s11082-014-9987-y